ISSN 0031-918X, Physics of Metals and Metallography, 2023, Vol. 124, No. 13, pp. 1472–1481. © Pleiades Publishing, Ltd., 2023.
ISSN 0031-918X, Physics of Metals and Metallography, 2023. © Pleiades Publishing, Ltd., 2023.

STRUCTURE, PHASE TRANSFORMATIONS, AND DIFFUSION

Electrochemical Properties of TiAl-Based Alloys

Y. Garip[a], * and O. Ozdemir[a]

[a] *Sakarya Applied Sciences University, Technology Faculty, Department of Metallurgy and Materials Engineering, Esentepe Campus, Sakarya, 54187 Turkey*

**e-mail: yigitgarip@hotmail.com*

Received April 14, 2023; revised July 26, 2023; accepted August 17, 2023

Abstract—TiAl alloys represent a promising potential for use in many fields including automotive, aerospace and marine industries. Therefore, it can be considered important to investigate the ability of these alloys to withstand such harsh environments. To this intended, the following study attempted to determine the electrochemical properties of Ti–48Al–2Mo–2(Cr,Mn) (at %) alloys in 3.5 wt % NaCl solution. The results of potentiodynamic polarization experiment revealed that Mo addition can enhance the corrosion resistance of the alloys, especially the Ti–48Al–2Cr alloy. Ti48Al–2Cr–2Mo was found to have the lowest corrosion rate value of 0.1153 mm/year, whereas Ti48Al–2Mn was found to have the highest corrosion rate value of 0.3952 mm/yr. The polarization resistance (R_p) of the alloys changes from 1.33 to 5.54 kΩ cm^2 depending on alloyed compositions. The electrochemical impedance spectroscopy (EIS) results confirmed that the corrosion behavior can be tailored through Mo addition. Accordingly, the best corrosion resistance belongs to the Ti48Al–2Cr–2Mo alloy, which presents the highest impedance value of 4.98×10^3 Ω. The surface morphologies of corroded alloys exhibited the pitting corrosion characteristics after the polarization experiments in 3.5 wt % NaCl solution. The number density of corrosion pits was significantly higher on the surfaces of the Ti48Al–2Mn and Ti48Al–2Mn–2Mo alloys. The enhanced corrosion resistance of Ti48Al–2Cr–2Mo alloy to NaCl solution is believed to be associated with the coupled positive effect of Cr and Mo in forming a surface film with a good protective ability. In addition, Ti48Al–2Cr–2Mo exhibited high resistance to NaCl solution at a level, which can be considered an optimum material for fabricating parts that serve in the marine environment.

Keywords: TiAl, NaCl solution, electrochemical behavior, alloying elements

DOI: 10.1134/S0031918X23600586

INTRODUCTION

In the past few decades, TiAl alloys have gathered significant interest from researchers who are committed to materials research and development in the academic community and industrial sectors because of their remarkable properties like low density (3.9–4.2 g cm^{-3}), high melting point, high specific yield strength, good creep properties as well as adequate oxidation and corrosion resistance [1–5]. The combination of all these unique properties makes TiAl alloys have a wide broad of engineering applications in the field of aerospace and automotive, especially they are considered suitable candidates for turbine blades in aero-gas turbines and turbocharger rotors in automotive engines [6]. One of the main qualities expected from materials driven by the demand to meet the current requirements in such application areas is resistance against chemically challenging mediums such as corrosive salt and acid solutions. Due to the growing demand for the design of TiAl alloys with excellent properties, many studies have been led to enhance the properties of these alloys, most of which are related to their mechanical [7–9] and oxidation [10–12] responses. However, according to the best of our knowledge, there are limited works available addressing the electrochemical behavior of TiAl alloys in various corrosive solutions, which puts forward more attention to be paid to the electrochemical properties of these alloys.

TiAl alloy designed by adding various alloying elements can be regarded as an effective approach to enhance the corrosion behavior of these alloys. Mo addition has been stated to play a leading role in enhancing the passivity and corrosion performance of Ti alloys [13, 14]. Mn and Cr additions were selected as alloying elements in this work because they have lower cost and higher availability as compared to other elements such as scarce Ta and Nb. However, Pardo et al. [15] have found that the addition of Mn into the austenitic stainless steel increases the corrosion rate in chloride-containing solution. Whereas, Cr addition has been reported to be beneficial for improved corrosion performance in acidic solutions [16]. Therefore, it is important to determine the effects of Mo, Mn and Cr alloying elements on the corrosion behavior of TiAl alloy in NaCl corrosive solution. To this end, the designed Ti–48Al–2Mo–2(Cr, Mn) alloy is believed

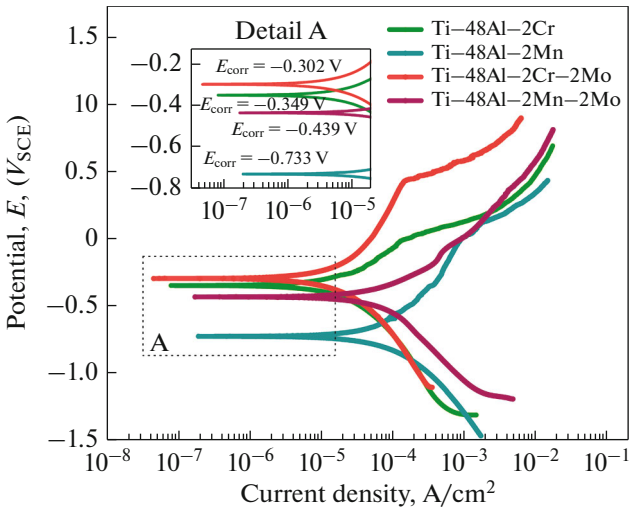

Fig. 1. The potentiodynamic polarization curves of TiAl alloys in 3.5 wt % NaCl solution.

to be a potential candidate to attain the intended perspective. This work addressed the role of Cr, Mn and Mo alloying elements on the electrochemical corrosion properties of TiA alloys in 3.5 wt % NaCl solution.

EXPERIMENTAL

Ti–48Al–2Mo–2(Cr,Mn) (at %) alloys investigated in this study were obtained through powder metallurgy merged with an electric current assisted sintering process (ECAS), the production details were provided in our previous study [4]. The electrochemical measurements were conducted on an electrochemical workstation (PCI4/750/ZRA, Gamry Instrument) with a standard three-electrode cell system. A saturated calomel electrode (SCE) served as a reference electrode (RE) and a graphite rod was the counter electrode (CE). The TiAl sample was adapted as a working electrode (WE) with a surface area of 0.785 cm^2, and the electrolyte was 3.5 wt % NaCl solution. All experiments were performed at room temperature. Potentiodynamic polarization curves were measured at a scan rate of 1 mV/s and the potential scanning range was from –1.5 to 0.9 V. After electrochemical measurements, tafel extrapolation technique on anodic and cathodic branches was applied to acquire the corrosion potential (E_{corr}) and the corrosion current density (I_{corr}). Electrochemical impedance spectroscopy (EIS) analyses were conducted at Open circuit potential (OCP) in the frequency ranging from 10^{-1} to 10^5 Hz. The surface morphology of corroded alloys was examined using a scanning electron microscope (SEM, JEOL JSM-6060, LV).

RESULTS AND DISCUSSION

The potentiodynamic polarization curves for all of the four TiAl alloys exposed in 3.5 wt % NaCl solution are illustrated in Fig. 1. These curves are quite beneficial for revealing some electrochemical parameters such as corrosion potential (E_{corr}), corrosion current density (I_{corr}), and Tafel constants (anodic polarisation (βa) and cathodic polarisation (βc)). The mentioned parameters in Table 1 are derived from the polarization curves by analyzing the linear part of the anodic and cathodic branches corresponding to the investigated alloys. As can be seen in Table 1, some shifts in the E_{corr} values and a notable difference in the I_{corr} values of the alloys are evident, which allows us to say that the corrosion resistance of TiAl alloys is affected by the addition of alloying elements. According to Table 1, E_{corr} values of the alloys are in the range from –0.733 to –0.302 V, while their I_{corr} values are in the range of 4.56×10^{-5} to 1.39×10^{-5} A/cm^2. For the sake of comparison, the E_{corr} of the TiAl–2Cr has shifted in a nobler direction compared to the TiAl–2Mn, and also the I_{corr} value is decreased by approximately 2.6 times for TiAl–2Cr, which implies that the addition of Cr into TiAl alloy improves the corrosion behavior more effectively. The noticeable effect of Cr element on the corrosion performance may correspond to its passivation behavior, which effect is consistent with increased E_{corr} and decreased I_{corr} values. It has been stated that the descending sequence of passivation ability is Cr, Ni, Co, Fe, Mn and Cu in the multicomponent alloys [17], providing an indication that the ability of Cr to form a protective film on the surface plays a crucial role in determining the corrosion tendency. Regarding the role of Mn addition on corrosion resistance of TiAl alloy, the effect of Mn on the corrosion property of Ti–24Nb–4Zr–xMn ($x = 0$, 1, 3, 5 wt %) alloy in Ringer's solution has been

Table 1. Electrochemical parameters of TiAl alloys exposed in 3.5 wt % NaCl solution

Alloys, at %	E_{corr}, V	I_{corr}, A/cm^2	β_a, V/dec	β_c, V/dec	R_p, kΩ cm^2
Ti–48Al–2Cr	–0.349	1.74×10^{-5}	0.288	–0.375	4.06
Ti–48Al–2Mn	–0.733	4.56×10^{-5}	0.329	–0.242	1.33
Ti–48Al–2Cr–2Mo	–0.302	1.39×10^{-5}	0.344	–0.367	5.54
Ti–48Al–2Mn–2Mo	–0.427	4.07×10^{-5}	0.255	–0.278	1.42

explored by Wu et al. [18]. Their electrochemical measurements revealed that the corrosion resistance is enhanced with the increase of Mn content. Though the enhanced corrosion resistance was attained by the addition of Mn, there was a slight improvement in the corrosion resistance, as reported in [18], for the alloy with 3 wt % Mn in comparison with the alloy without Mn. However, the prevailing tendency of Cr element in decreasing corrosion rate overshadowed the effect of Mn element on the alloys examined in this work when the E_{corr} and I_{corr} values corresponding to the alloys are co-considered. As for the TiAl alloys with the addition of Mo, the Mo element seems to play a beneficial role in increasing the corrosion resistance of the alloys, based on the results presented in Table 1. It can be noticed that Mo addition exerts significant effects on the E_{corr} and I_{corr} of the alloys compared to those found for the alloys without Mo addition. Moreover, among the four alloys examined, TiAl–Cr–Mo alloy shows the best corrosion behavior with the lowest value of I_{corr} and the highest value of E_{corr} under the experimental conditions used in this work. A similar explanation may also hold good for TiAl–Mn–Mo alloy, as an improvement in corrosion resistance of TiAls is noted with an increase in E_{corr} and a deccrease in I_{corr}. The results presented above corresponding to the effect of Mo addition are consistent with the statement that Mo content increases the corrosion resistance of Ti alloys with various compositions [14, 19], in which corrosion results of the alloys characterized by electrochemical measurements confirmed that Mo lowers the corrosion rate of the Ti alloys to a level comparable to that of pure Ti.

In order to present the readers an insight into the general corrosion tendency of TiAl alloys investigated in this work, a comparison including the I_{corr} and E_{corr} values of Ti alloys with various compositions [20–24] was performed in Fig. 2. From the comparison in Fig. 2, it can be concluded that the mentioned data of the studied alloys lie close to those reported in the literature, except for [20, 21].

Moreover, polarization resistance (R_p) is considered a considerable parameter in characterizing the corrosion resistance of the materials. R_p can be calculated using the following equation [25]:

$$R_p = \frac{\beta_a \beta_c}{2.303 i_{corr} (\beta_a + \beta_c)}. \quad (1)$$

Table 1 presents the obtained R_p values corresponding to the TiAl alloys, and their R_p values change from 1.33 to 5.54 kΩ cm^2 depending on the designed compositions. R_p is inversely proportional to the corrosion rate, that is to say, the greater R_p value is, the slower the corrosion rate is. With alloying elements variation, the corrosion resistance can be ranked as: TiAl–Mn < TiAl–Mn–Mo < TiAl–Cr < TiAl–Cr–Mo under the selected experimental conditions, which

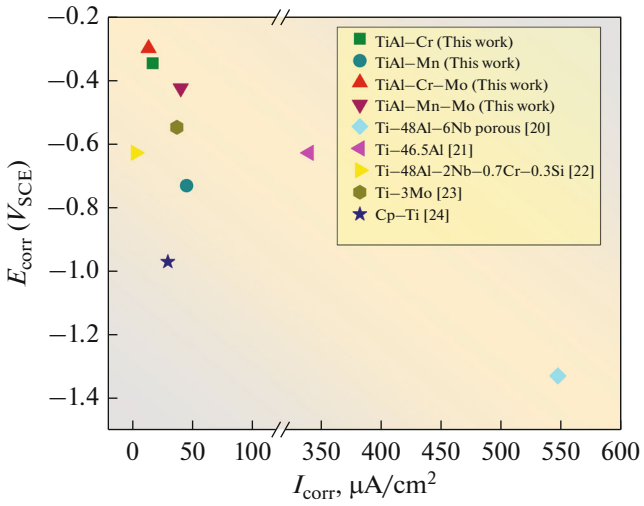

Fig. 2. Comparison of I_{corr} and E_{corr} of investigated alloys and Ti alloys with various compositions in 3.5 wt % NaCl solution.

is in line with the polarization curves from Fig. 1, where the best corrosion behavior is found for TiAl–Cr–Mo alloy. However, the electrochemical parameters derived from the polarization curves may not always be satisfactory to determine the corrosion properties of materials. In this regard, the function of atomic-fraction-weighted values of atomic weight, the density of the alloy and ion valence also have to be taken into account to reveal the corrosion rate (R_{corr}). Thus, the following equation can be considered to calculate the general corrosion rate (R_{corr}) of the alloys [26]:

$$R_{corr} = 0.00327 (I_{corr} EW)/D, \quad (2)$$

where R_{corr} is the corrosion rate (mm/year), I_{corr} is the corrosion current density (μA/cm^2), EW is the equivalent weight and D is the density (g/cm^3). EW can be estimated as follows:

$$EW = \left(\sum \frac{f_i n_i}{A_i} \right)^{-1}, \quad (3)$$

where f_i, n_i and A_i represent the mass fraction, electrons exchanged, and atomic weight, respectively, of the ith alloying elements. The obtained R_{corr} values for the TiAl alloys are put forward in Fig. 3, in which the lowest one is found for the TiAl–Cr–Mo (0.1153 mm/yr) and the highest one is found for the TiAl–Mn (0.3952 mm/yr). The TiAl alloy having Cr and Mo additions has the highest corrosion resistance due to the fact that a low value of R_{corr} is associated with high corrosion resistance. In the case of TiAl–Cr alloy, the removal of Mo element from TiAl–Cr–Mo alloy brought up the value of R_{corr} to 0.1514 mm/yr, which has the second-lowest value. Compared to TiAl–Cr, the corrosion resistance of TiAl–Cr–Mo increased by 24%. However, when Mo is absent from

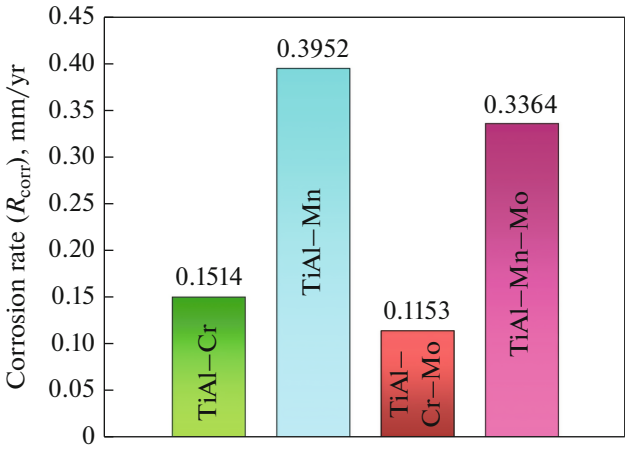

Fig. 3. R_{corr} values of TiAl alloys exposed in 3.5 wt % NaCl solution.

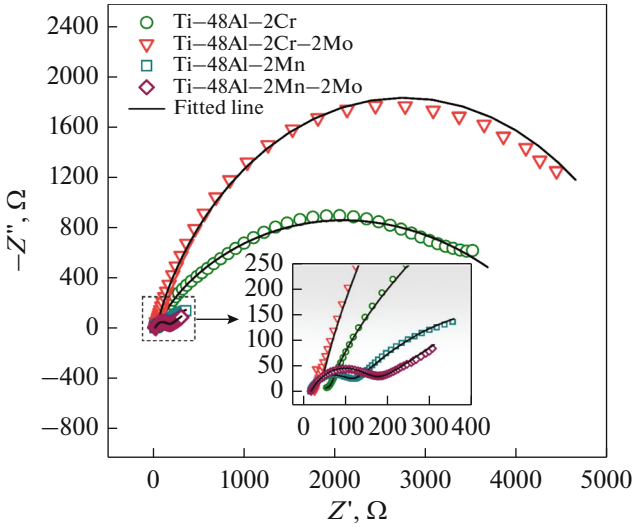

Fig. 4. Nyquist plots and fitted lines of TiAl alloys in 3.5% NaCl solution. The insert indicates the details of the Nyquist plots.

the TiAl–Mn alloy, the alloy experiences the highest corrosion rate, and its value of R_{corr} is noticed to be much higher, corresponding to 0.3952 mm/year, which represents around 15% deterioration in corrosion resistance compared to that observed for TiAl–Mn–Mo. One can be seen that Mo addition yields a positive effect on the corrosion behavior of both alloys, i.e. TiAl–Cr and TiAl–Mn, however, it should be noted that Mo reveals a stronger influence on the former. Anti-corrosion ability of Mo addition was attributed to the presence of Mo^{6+} ions in the passive film constituted on the surface, making it more stable against degradation induced by the invasion of aggressive Cl^- ions. Furthermore, the addition of Mo was reported to be responsible for the improvement of the repassivation behavior of the alloy [15]. In line with the reported findings, the better corrosion resistance caused by the addition of Mo is likely to be as a result of the passive film formed on the TiAl alloys being more stable to Cl^- ions attacks. At the same time, the microstructure-property relations of the alloys can present meaningful results regarding their corrosion behaviors. According to [4], all of the alloys were made up of TiAl and Ti_3Al phases, namely, the alloying process did not affect the phase constituents of TiAls. Besides that, as dissimilar to those of other TiAls, TiAl phase in the microstructures of both Mo-containing alloys was Mo-rich. Consequently, this may explain why Mo-containing TiAl alloys have enhanced corrosion resistance.

The electrochemical impedance spectroscopy (EIS) studies were conducted to shed more light on the electrochemical properties of the alloys and to further understand the electrochemical reactions that emerged at the electrode/electrolyte interface in 3.5 wt % NaCl solution. Accordingly, the measured Nyquist data for the TiAl alloys are plotted in Fig. 4 and the corresponding Bode plots are presented in Fig. 5. At first sight at the Nyquist spectra shown in Fig. 4, the curves are observed to consist of unfinished semi-arcs with their centers depressed below the x-axis. This observation is typically featured in the non-perfect capacitive behavior of the surface [27]. The curves of TiAl–Cr and TiAl–Cr–Mo alloys appear to have a similar shape. To be more specific, the Nyquist spectra of these alloys include one capacitive loop from high to low frequency, each of which has a different semi-arc diameter. The observed one capacitive loop in Fig. 4 corresponding to TiAl–Cr and TiAl–Cr–Mo alloys indicates the presence of one time constant. However, clearly from Fig. 4, two capacitive loops at high and low frequency ranges can be observed for the Nyquist spectra of TiAl–Mn and TiAl–Mn–Mo alloys, signifying the existence of two capacitive time constants. It can be inferred that a different corrosion behavior is valid for these alloys compared to TiAl–Cr and TiAl–Cr–Mo alloys, in that the corresponding Nyquist curves include two capacitive loops with reduced diameters. The appearance of two capacitive loops has been reported to be associated with the severe degradation of corrosion resistance, ascribed to the formation of a porous surface film [28]. The diameters of the semi-arcs for TiAl alloys in Nyquist plots evidently differ. The largest semi-arc diameter is observed for TiAl–Cr–Mo alloy. Further, a decrease in the diameter of the semi-arc is noted for the TiAl–Cr alloy due to the removal of Mo element from TiAl. Dissimilar to what is observed on the TiAl–Cr and TiAl–Cr–Mo alloys, the remaining alloys, i.e., TiAl–Mn and TiAl–Mn–Mo, on the other hand, appear to present similar features with reduced diameters of the semi-arcs, with TiAl–Mn–Mo being slightly larger than TiAl–Mn in terms of semi-arc diameter. Another point worth noting is the coupled

effect of Cr and Mo is much more prominent than that of Mn and Mo, as evidenced in Fig. 4 by the EIS results. Such a result may be an indication that both alloys are governed by different corrosion mechanisms. This is remarkable in terms of the corrosion performances of alloys. The diameter of the semi-arc in Nyquist plots provides a useful indication for the fact about alloying element-induced improvement of the corrosion resistance of TiAl alloys. That is to say, the larger the diameter of the semi-arc is, the higher the corrosion resistance of the alloys [29], further indicating that the occurrence of a low corrosion rate is represented by greater impedance values at lower frequency in the Bode plot. In view of this consideration, a comparison of semi-arc sizes of four TiAl alloys points out that TiAl–Cr–Mo alloy owns the largest semi-arc size, representing the best corrosion performance. This evidence affirms that the presence of Mo significantly increases the corrosion resistance of TiAl–Cr alloy in NaCl solution, as can be seen in Fig. 4. Moreover, enhanced resistance signifies that chemical reactions will be more difficult to happen in the surface film of the TiAl–Cr–Mo alloy during the corrosion process. When this comparison is made with those observed in Mn-containing alloys, it is clearly visible that the alloys have a much smaller semi-arc size, which characterizes these alloys as more susceptible to corrosion under the same experimental conditions. A lower corrosion performance for the case of TiAl–Mn and TiAl–Mn–Mo alloys is most likely a manifestation of the weakened protective ability of surface film. The Nyquist plot evidently confirms that alloying elements can play a role as a determining factor in the corrosion performance of TiAl alloys. Additionally, it is worth emphasizing that the observed trend is in line with the corrosion results inferred from the polarization curves presented in Fig. 1.

Bode spectra with Bode-phase and Bode-magnitude plots for TiAl alloys are presented in Fig. 5. The phase angles of the alloys drop to near zero degrees at high frequencies, indicating that the impedance is governed by electrolyte resistance in this frequency range. In the medium-frequency region, the phase angles corresponding to the alloys rise and attain their own maximum values. Among the alloys investigated, TiAl–Cr–Mo alloy possesses the highest phase angle corresponding to about 65°, while the TiAl–Cr alloy takes second place with a phase angle of about 45°. It can be observed that the Bode-phase and Bode-magnitude plots are similar for TiAl–Mn and TiAl–Mn–Mo alloys. The smallest phase angle is observed for these two alloys. Furthermore, unlike those of TiAl–Cr and TiAl–Cr–Mo alloys, two peaks can be noticed in the Bode phase plots of TiAl–Mn and TiAl–Mn–Mo alloys, which attribute to the appearance of two-time constants. The effects of alloying elements on the Bode plots can determine the corrosion resistance of

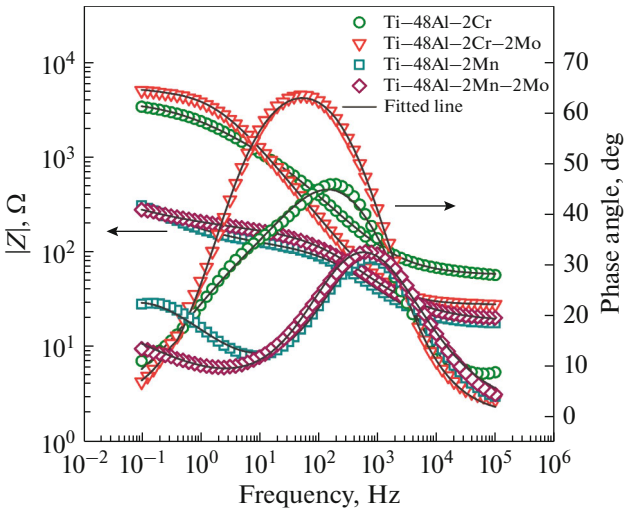

Fig. 5. Bode plots and fitted lines of TiAl alloys in 3.5% NaCl solution.

the alloys. To be specific: the higher values of impedance and maximum phase angle correspond to better corrosion resistance. The impedance value ($|Z|$) at a fixed frequency of 0.1 Hz in the Bode-magnitude plots is an effective tool for the evaluation of the corrosion performance of the alloy [30]. As shown in Fig. 5, the impedance values at 0.1 Hz for the TiAl alloys are in descending order as follows: TiAl–Cr–Mo > TiAl–Cr > TiAl–Mn–Mo ≅ TiAl–Mn. Accordingly, the best corrosion resistance belongs to the TiAl–Cr–Mo alloy, which presents the highest impedance value of $4.98 \times 10^3\ \Omega$.

The EIS results are fitted using the equivalent electrical circuit (EEC) models to further analysis of the Bode spectra. Two different EEC models are applied to fit the EIS results of the TiAl alloys, as shown in Figs. 6a, 6b. Model A comprises the R_s connected in series with a parallel combination of a constant phase element (CPE, Q) and an R_{ct}, where R_s is the electrolyte resistance, CPE is associated with the capacitance of the surface film and R_{ct} is the charge transfer resistance. Model B shows that the R_s is connected in series with four elements, as can be monitored in Fig. 6b. This adopted EEC model consists of two-time constants; the first of which corresponds to the high-frequency time constant (Q_f) and is associated with the defective corrosion film formed on the alloy and the latter of which is the low-frequency time constant (Q_{dl}) representing the charge transfer process that occurred on the surface of alloy [31]. In this model, the paralleled Q_f–R_f refer to the surface film capacitance and surface film resistance, respectively. The paralleled Q_{dl}–R_{ct}, which is connected in series with R_f, corresponds to the capacitance of the double layer and charge transfer resistance, respectively. The CPE is introduced instead of the ideal capacitance element

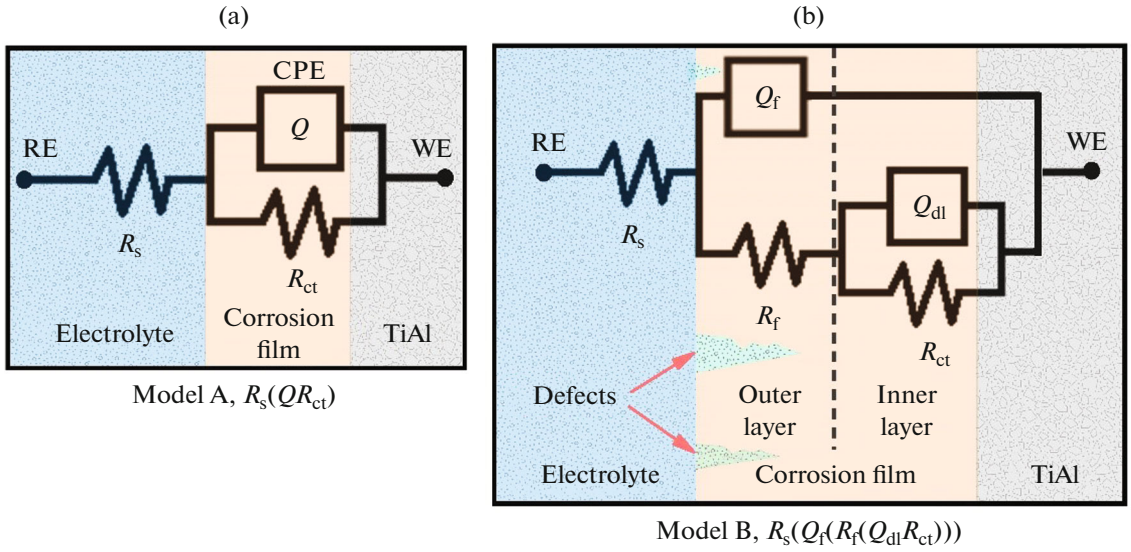

Fig. 6. The equivalent electrical circuits for fitting the EIS data of the TiAl alloys, (a) Ti48Al–2Cr and Ti48Al–2Cr–2Mo, (b) Ti48Al–2Mn and Ti48Al–2Mn–2Mo.

due to the inhomogeneous surfaces and adsorption effects. The CPE impedance (Z_{CPE}) can be described as follows [32]:

$$Z_{CPE} = \frac{1}{Y_0}(j\omega)^{-n}, \quad (4)$$

where Y_0 is the admittance magnitude of the CPE, j is the imaginary unit, and ω is the angular frequency. The value of n describes the deviation from the ideal capacitive behavior, which changes from 0 to 1. When the n is 0, the CPE denotes an ideal resistor; when the n is 1, it describes an ideal capacitor; when the n is 0.5, it behaves as a Warburg impedance [29].

Table 2 presents the fitting parameter values of the electrochemical impedance data. From Table 2, the chi-square (λ^2) values are found to be lying in the range of 10^{-3} to 10^{-4}, indicating that it can be considered to be good fitting quality. The total resistance in the proposed circuits determines the corrosion performance of the alloys. The total resistance of TiAl–Cr and TiAl–Cr–Mo alloys corresponds to R_{ct} in model A, while that of TiAl–Mn and TiAl–Mn–Mo alloys equals to $R_f + R_{ct}$ in model B. A higher resistance reflects a lower electrochemical reaction rate, which is responsible for enhanced corrosion resistance. It can be clearly noticed from Table 2 that the resistance values of TiAl–Cr and TiAl–Cr–Mo alloys are much higher than the remaining two alloys. Accordingly, the corrosion film formed on TiAl–Cr–Mo alloy has the best protective ability, while that formed on TiAl–Mn alloy exhibits the worst.

The value of Q_f associated with the active area can provide evidence of the roughness of the corrosion film [33]. That is, the higher Q_f value of TiAl–Mn alloy makes its corrosion film rougher as compared to TiAl–Mn–Mo alloy. Additionally, the R_{ct} values are higher than the R_f values in both cases, suggesting that

Table 2. Values of the electrical equivalent circuit (EEC) fitting parameters for EIS data of TiAl alloys in 3.5% NaCl solution

Fitting parameters	Ti–48Al–2Cr	Ti–48Al–2Cr–2Mo	Ti–48Al–2Mn	Ti–48Al–2Mn–2Mo
R_s, Ω cm^2	27.25	33.78	16.58	18.14
Q_f, Ω^{-1} cm^{-2} s^n	–	–	2.86×10^{-5}	2.05×10^{-5}
n_f	–	–	0.88	0.90
R_f, Ω cm^2	–	–	42.9	75.3
Q_{dl}, Ω^{-1} cm^{-2} s^n	6.32×10^{-5} (Q_{CPE})	3.61×10^{-5} (Q_{CPE})	1.47×10^{-5}	1.39×10^{-5}
n_{dl}	0.83 (n_{CPE})	0.89 (n_{CPE})	0.83	0.78
R_{ct}, Ω cm^2	3645.2	5651.6	162.3	214.6
Chi-square (λ^2)	2.14×10^{-3}	4.41×10^{-3}	1.28×10^{-4}	2.76×10^{-4}

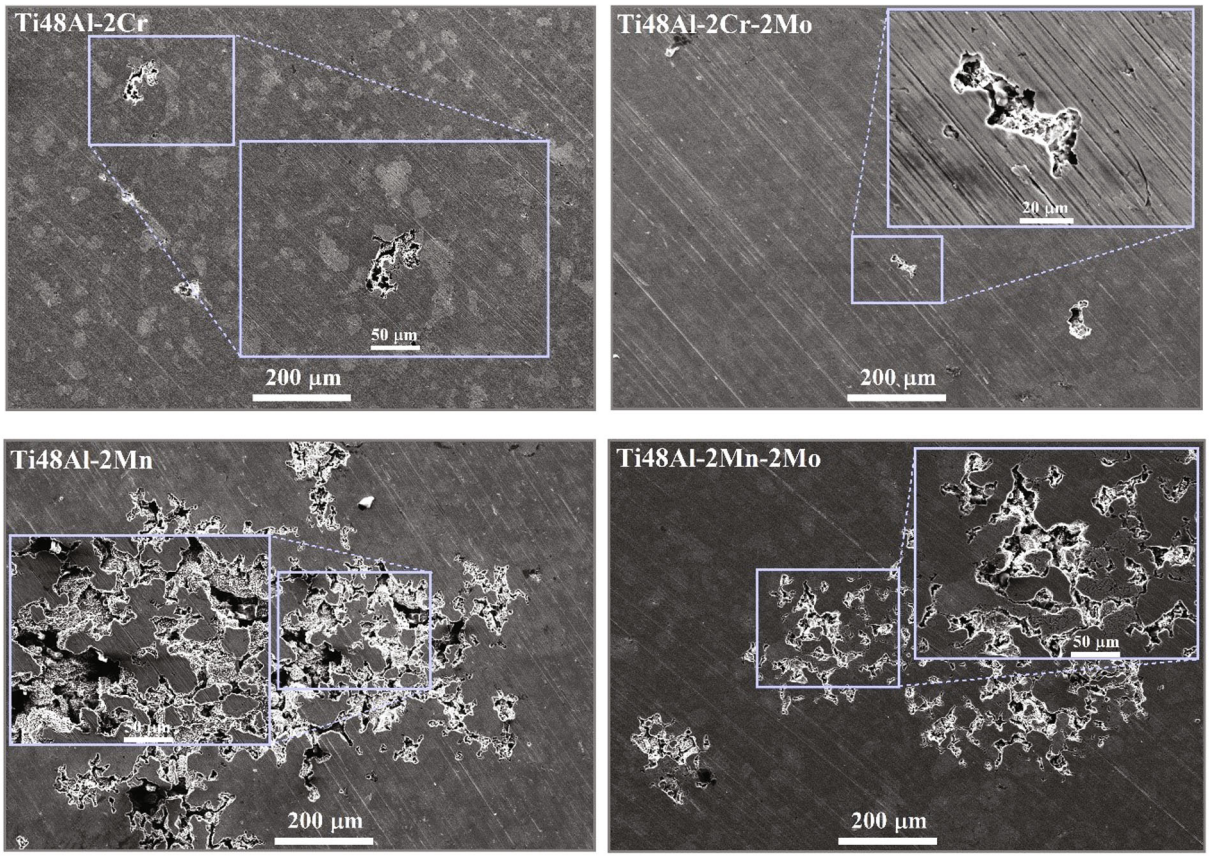

Fig. 7. Surface morphologies of TiAl alloys after potentiodynamic polarization tests in 3.5 wt % NaCl solution.

the inner layer presents a better resistance to chloride attacks.

SEM studies were performed to observe the results of the responses of TiAl alloys to NaCl solution. Figure 7 put forwards the surface morphologies (Secondary electron imaging (SEI)) of the alloys after the polarization tests in 3.5 wt % NaCl solution. Many corrosion pits with different shapes and sizes are clearly visible on corroded surfaces of all alloys, which are especially notable for the TiAl–Mn and TiAl–Mn–Mo alloys. It should be mentioned that the microstructures are represented by two different phases; the first region which is dark gray belongs to the TiAl phase and the second one is the light gray region which corresponds to the Ti_3Al phase. In the binary TiAl system, the Ti_3Al (α_2) phase contains 22–39 (at %) Al, while the TiAl (γ) phase has Al content between 48.5 and 66 (at %) [34]. In addition to these phases, Mo-containing TiAl alloys have also TiAl phases that are rich in Mo. The composition of Mo-rich phases was reported to be 49.4Ti–43.1Al–2.1Cr–5.4Mo for TiAl–Cr–Mo alloy and 41.1Ti–52.8Al–1.4Mn–4.7Mo (at %) for TiAl–Mn–Mo alloy [4]. According to Fig. 7, the Ti_3Al phase appears to be more prone to corrosion because most of the corrosion pits are distributed upon it. Thus, this reveals that the corrosion damage occurred more dramatically for the Ti_3Al phase. This fact may be an indication that the Ti_3Al phase is damaged as a result of selective corrosion. However, the effect of O^- and Cl^- ions on the corrosion process of TiAl and Ti_3Al phases needs to be further investigated. On the other hand, Fig. 7 confirms that the alloying strategy has a central role in affecting the number density of corrosion pits. TiAl–Cr and TiAl–Cr–Mo alloys are inferred to have enhanced surface morphology as compared to the remaining alloys due to the fact that they show the tendency of decreasing the number of corrosion pits. Moreover, the size and depth of the pitting holes on the surface of both mentioned alloys are smaller than those of TiAl–Mn and TiAl–Mn–Mo alloys, indicating that the alloys have different passivation characteristics. A study has been reported by Wu et al. [35], which highlighted that a thicker passive film was effective in ameliorating the pitting resistance of steel in chloride electrolyte. However, the aggressive chloride ions attack the corrosion film constituted on the surface and attempt to break it down, and once the passive film is damaged, pit nucleation and growth occur more easily on the surface. It has been proposed that Mo may play an important role in more than one step in a pitting process. Mo element changes the polarity

of the passive film by the formation of insoluble Mo compounds: the appearance of MoO^{n-} ions in the outmost part of the passive film modifies its intrinsically anionic selectivity into a cationic one, producing the development of a bipolar layer [15]. It encourages the diffusion of O^{2-}, and hence Cr_2O_3 formation [36–39] and also impedes Cl^- entrance making the passive film more stable against corrosion attacks [40]. Moreover, Mo facilitates the repassivation behavior and blocks the growth of corrosion pits [38, 41]. The results of the work performed by Ilevbare and Burstein [41] featured that additional Mo to the stainless steel lowered the number and size of both nucleation and metastable pits, reducing the probability of forming stable corrosion pits. The literature data showing that the Mo element presents better protection from Cl^- attack which confirms the results of our study. Additionally, the accounted for possible mechanisms behind the positive effect of Mo addition are also thought to hold true for the alloys investigated here.

CONCLUSIONS

In this work, the corrosion properties of four series of TiAl alloys with the compositions of Ti–48Al–2Cr, Ti–48Al–2Mn, Ti–48Al–2Cr–2Mo and Ti–48Al–2Mn–2Mo in 3.5 wt % NaCl solution were comparatively studied through electrochemical techniques. The corrosion behaviors of these alloys were observed to be significantly affected by Cr, Mn and Mo additions. The following main conclusions can be drawn from the above work:

(1) Mn addition showed a harmful effect on the corrosion resistance of TiAl alloy investigated in 3.5 wt % NaCl solution. Its presence dramatically increased the corrosion rate of the alloy, reaching the highest R_{corr} value of 0.3952 mm/year as well as the lowest R_p value of 1.33 kΩ cm^2.

(2) With the addition of Mo, TiAl alloys exhibited an improved corrosion performance, and TiAl–Cr–Mo alloy presented the highest corrosion resistance to NaCl solution, with the least R_{corr} value of 0.1153 mm/yr.

(3) TiAl–Cr–Mo alloy offered good corrosion resistance, exhibiting a higher phase angle, larger semi-arc diameter, and greater charge transfer resistance (R_{ct}), which could be determined by the electrochemical impedance spectroscopy (EIS) tests.

(4) The corroded surfaces bore the features of pitting corrosion. In the case of TiAl–Mn and TiAl–Mn–Mo alloys, the number density of corrosion pits was significantly higher.

FUNDING

This work was supported by ongoing institutional funding. No additional grants to carry out or direct this particular research were obtained.

CONFLICT OF INTEREST

The authors of this work declare that they have no conflicts of interest.

REFERENCES

1. Y. Garip, "Investigation of isothermal oxidation performance of TiAl alloys sintered by different processing methods," Intermetallics **127**, 106985 (2020). https://doi.org/10.1016/j.intermet.2020.106985
2. V. A. C. Haanappel and M. F. Stroosnijder, "The effect of ion implantation on the oxidation behaviour of TiAl-based intermetallic alloys at 900°C," Surf. Coat. Technol. **105**, 147–154 (1998). https://doi.org/10.1016/s0257-8972(98)00472-1
3. Y. Garip, Z. Garip, and O. Ozdemir, "Prediction modeling of Type-I hot corrosion performance of Ti–Al–Mo–X (X = Cr, Mn) alloys in $(Na,K)_2SO_4$ molten salt mixture environment at 900°C," J. Alloys Compd. **843**, 156010 (2020). https://doi.org/10.1016/j.jallcom.2020.156010
4. Y. Garip and O. Ozdemir, "Corrosion behavior of the resistance sintered TiAl based intermetallics induced by two different molten salt mixture," Corros. Sci. **174**, 108819 (2020). https://doi.org/10.1016/j.corsci.2020.108819
5. Y. Garip and O. Ozdemir, "Comparative study of the oxidation and hot corrosion behaviors of TiAl–Cr intermetallic alloy produced by electric current activated sintering," J. Alloys Compd. **780**, 364–377 (2019). https://doi.org/10.1016/j.jallcom.2018.11.324
6. L.-K. Wu, J.-J. Wu, W.-Ya. Wu, F.-H. Cao, and M.-Ya. Jiang, "Sol–gel-based coatings for oxidation protection of TiAl alloys," J. Mater. Sci. **55**, 6330–6351 (2020). https://doi.org/10.1007/s10853-020-04466-0
7. X. Zhang, C. Li, M. Zheng, X. Yang, Z. Ye, and J. Gu, "Chemical, microstructure, and mechanical property of TiAl alloys produced by high-power direct laser deposition," J. Mater. Sci. Technol. **117**, 99–108 (2022). https://doi.org/10.1016/j.jmst.2021.07.062
8. D. Wimler, J. Lindemann, T. Kremmer, H. Clemens, and S. Mayer, "Microstructure and mechanical properties of novel TiAl alloys tailored via phase and precipitate morphology," Intermetallics **138**, 107316 (2021). https://doi.org/10.1016/j.intermet.2021.107316
9. V. M. Imayev, A. A. Ganeev, D. M. Trofimov, N. Ju. Parkhimovich, and R. M. Imayev, "Effect of Nb, Zr and Zr + Hf on the microstructure and mechanical properties of β-solidifying γ-TiAl alloys," Mater. Sci. Eng., A **817**, 141388 (2021). https://doi.org/10.1016/j.msea.2021.141388
10. J. Małecka, W. Grzesik, and A. Hernas, "An investigation on oxidation wear mechanisms of Ti–46Al–7Nb–0.7Cr–0.1Si–0.2Ni intermetallic-based alloys," Corros. Sci. **52**, 263–272 (2010). https://doi.org/10.1016/j.corsci.2009.09.015
11. M. Bik, A. Gil, M. Stygar, J. Dąbrowa, P. Jeleń, E. Długoń, M. Leśniak, and M. Sitarz, "Studies on the oxidation resistance of SiOC glasses coated TiAl alloy,"

Intermetallics **105**, 29–38 (2019). https://doi.org/10.1016/j.intermet.2018.09.014

12. D. J. Kim, D. Y. Seo, H. Saari, T. Sawatzky, and Y.-W. Kim, "Isothermal oxidation behavior of powder metallurgy beta gamma TiAl–2Nb–2Mo alloy," Intermetallics **19**, 1509–1516 (2011). https://doi.org/10.1016/j.intermet.2011.05.027
13. J. E. G. González and J. C. Mirza-Rosca, "Study of the corrosion behavior of titanium and some of its alloys for biomedical and dental implant applications," J. Electroanal. Chem. **471**, 109–115 (1999). https://doi.org/10.1016/S0022-0728(99)00260-0
14. N. T. C. Oliveira and A. C. Guastaldi, "Electrochemical stability and corrosion resistance of Ti–Mo alloys for biomedical applications," Acta Biomater. **5**, 399–405 (2009). https://doi.org/10.1016/j.actbio.2008.07.010
15. A. Pardo, M. C. Merino, A. E. Coy, F. Viejo, R. Arrabal, and E. Matykina, "Pitting corrosion behaviour of austenitic stainless steels–Combining effects of Mn and Mo additions," Corros. Sci. **50**, 1796–1806 (2008). https://doi.org/10.1016/j.corsci.2008.04.005
16. C.-O. A. Olsson and D. Landolt, "Passive films on stainless steels—chemistry, structure and growth," Electrochim. Acta **48**, 1093–1104 (2003). https://doi.org/10.1016/s0013-4686(02)00841-1
17. R.-F. Zhao, B. Ren, B. Cai, Zh.-X. Liu, G.-P. Zhang, and J.-J. Zhang, "Corrosion behavior of CoxCrCuFeMnNi high-entropy alloys prepared by hot pressing sintered in 3.5% NaCl solution," Results Phys. **15**, 102667 (2019). https://doi.org/10.1016/j.rinp.2019.102667
18. J. Wu, X. Tan, X. An, J. Zhang, Yi. Guo, J. Liu, Yu. Luo, W. Yao, Q. Kong, and Q. Wang, "Development of biomedical Ti–Nb–Zr–Mn alloys with enhanced mechanical properties and corrosion resistance," Mater. Today Commun. **30**, 103027 (2022). https://doi.org/10.1016/j.mtcomm.2021.103027
19. P. F. Santos, M. Niinomi, H. Liu, K. Cho, M. Nakai, A. Trenggono, S. Champagne, H. Hermawan, and T. Narushima, "Improvement of microstructure, mechanical and corrosion properties of biomedical Ti–Mn alloys by Mo addition," Mater. Des. **110**, 414–424 (2016). https://doi.org/10.1016/j.matdes.2016.07.115
20. W. Gui, J. Lin, M. Liu, Yu. Qu, Yu. Wang, and Yo. Liang, "Effects of nano-NiO addition on the microstructure and corrosion properties of high Nb–TiAl alloy," J. Alloys Compd. **782**, 973–980 (2019). https://doi.org/10.1016/j.jallcom.2018.12.200
21. C. Liao, J. Yang, Yu. He, and X. Ming, "Electrochemical corrosion behavior of the carburized porous TiAl alloy," J. Alloys Compd. **619**, 221–227 (2015). https://doi.org/10.1016/j.jallcom.2014.08.021
22. S. Magogodi, M. Mathabathe, A. Bolokang, and C. Siyasiya, "The electrochemical corrosion behaviour of Ti–48Al–2Nb–0.7Cr–0.3Si alloy in 3.5% NaCl," MATEC Web Conf. **370**, 06008 (2022). https://doi.org/10.1051/matecconf/202237006008
23. Z. Pan, Ya. Wei, Yu. Fu, H. Luo, and X. Li, "Effect of electrochemical hydrogen charging on the mechanical property and corrosion behavior of Ti–3Mo alloy," Corros. Sci. **200**, 110219 (2022). https://doi.org/10.1016/j.corsci.2022.110219
24. H. Nady, M. M. El-Rabiei, and M. Samy, "Corrosion behavior and electrochemical properties of carbon steel, commercial pure titanium, copper and copper–aluminum–nickel alloy in 3.5% sodium chloride containing sulfide ions," Egyptian J. Pet. **26**, 79–94 (2017). https://doi.org/10.1016/j.ejpe.2016.02.008
25. T. Xia, L. Zeng, X. Zhang, J. Liu, W. Zhang, T. Liang, and B. Yang, "Enhanced corrosion resistance of a Cu 10Ni alloy in a 3.5 wt % NaCl solution by means of ultrasonic surface rolling treatment," Surf. Coat. Technol. **363**, 390–399 (2019). https://doi.org/10.1016/j.surfcoat.2019.02.039
26. Y. Garip, N. Ergin, and O. Ozdemir, "Resistance sintering of $CoCrFeNiAl_x$ ($x = 0.7$, 0.85, 1) high entropy alloys: Microstructural characterization, oxidation and corrosion properties," J. Alloys Compd. **877**, 160180 (2021). https://doi.org/10.1016/j.jallcom.2021.160180
27. P. Muangtong, R. M. Namus, and R. Goodall, "Improved tribocorrosion resistance by addition of Sn to CrFeCoNi high entropy alloy," Metals **11**, 13 (2021). https://doi.org/10.3390/met11010013
28. B. Su, B. Wang, L. Luo, L. Wang, Ya. Su, Ya. Xu, F. Wang, B. Han, H. Huang, J. Guo, and H. Fu, "Effect of zirconium content on the microstructure and corrosion behavior of as-cast Ti–Al–Nb–Zr–Mo alloy," J. Mater. Res. Technol. **15**, 4896–4913 (2021). https://doi.org/10.1016/j.jmrt.2021.10.102
29. W.-R. Zhang, W.-B. Liao, P. Liaw, J.-L. Ren, J. Brechtl, and Yo. Zhang, "Effects of transient thermal shock on the microstructures and corrosion properties of a reduced activation high-entropy alloy," J. Alloys Compd. **918**, 165762 (2022). https://doi.org/10.1016/j.jallcom.2022.165762
30. P. Wang, Ya. Wang, F. Cui, X. Yang, A. Pan, and W. Wu, "Microstructural evolution, mechanical properties and corrosion resistance of $CoCrFeNiW_{0.5}$ high entropy alloys with various annealing heat treatment," J. Alloys Compd. **918**, 165602 (2022). https://doi.org/10.1016/j.jallcom.2022.165602
31. Zh.-Ch. Zhang, A.-D. Lan, M. Zhang, and J.-W. Qiao, "Effect of Ce on the pitting corrosion resistance of non-equiatomic high-entropy alloy $Fe_{40}Mn_{20}Cr_{20}Ni_{20}$ in 3.5 wt % NaCl solution," J. Alloys Compd. **909**, 164641 (2022). https://doi.org/10.1016/j.jallcom.2022.164641
32. X. Yan, H. Guo, W. Yang, S. Pang, Q. Wang, Y. Liu, P. Liaw, and T. Zhang, "$Al_{0.3}Cr_xFeCoNi$ high-entropy alloys with high corrosion resistance and good mechanical properties," J. Alloy Comp **860**, 158436 (2021). https://doi.org/10.1016/j.jallcom.2022.165762
33. K.-M. Hsu and Ch.-S. Lin, "Microstructural and electrochemical characterization of the passive film on a 50-kg hot rolled FeCrNiCoMn high entropy alloy," Mater. Today Commun. **26**, 101979 (2021). https://doi.org/10.1016/j.mtcomm.2020.101979
34. K. Kothari, R. Radhakrishnan, and N. M. Wereley, "Advances in gamma titanium aluminides and their manufacturing techniques," Prog. Aerosp. Sci. **55**, 1–16 (2012). https://doi.org/10.1016/j.paerosci.2012.04.001

35. M. Wu and J. Shi, "Beneficial and detrimental impacts of molybdate on corrosion resistance of steels in alkaline concrete pore solution with high chloride contamination," Corros. Sci. **183**, 109326 (2021). https://doi.org/10.1016/j.corsci.2021.109326

36. C. R. Clayton and Y. C. Lu, "A bipolar model of the passivity of stainless steels—III. The mechanism of MoO_4^{2-} formation and incorporation," Corros. Sci. **29**, 881–898 (1989). https://doi.org/10.1016/0010-938x(89)90059-0

37. M. A. Ameer, A. M. Fekry, and F. El-Taib Heakal, "Electrochemical behaviour of passive films on molybdenum-containing austenitic stainless steels in aqueous solutions," Electrochim. Acta **50**, 43–49 (2004). https://doi.org/10.1016/j.electacta.2004.07.011

38. W. J. Tobler and S. Virtanen, "Effect of Mo species on metastable pitting of $Fe_{18}Cr$ alloys—A current transient analysis," Corros. Sci. **48**, 1585–1607 (2006). https://doi.org/10.1016/j.corsci.2005.05.049

39. J. M. Bastidas, C. L. Torres, E. Cano, and J. L. Polo, "Influence of molybdenum on passivation of polarised stainless steels in a chloride environment," Corros. Sci. **44**, 625–633 (2002). https://doi.org/10.1016/s0010-938x(01)00072-5

40. K. Sugimoto and Y. Sawada, "The role of molybdenum additions to austenitic stainless steels in the inhibition of pitting in acid chloride solutions," Corros. Sci. **17**, 425–445 (1977). https://doi.org/10.1016/0010-938x(77)90032-4

41. G. O. Ilevbare and G. T. Burstein, "The role of alloyed molybdenum in the inhibition of pitting corrosion in stainless steels," Corros. Sci. **43**, 485–513 (2001). https://doi.org/10.1016/s0010-938x(00)00086-x